Development of a novel ReaxFF reactive potential for organochloride molecules

Matthieu Wolf, Didier Bégué, Germain Salvato Vallverdu

Development of a novel ReaxFF reactive potential for organochloride molecules

Matthieu Wolf,[1] Didier Bégué,[1] and Germain Salvato Vallverdu[1]

Universite de Pau et des Pays de l'Adour, E2S UPPA, CNRS, IPREM, UMR 5254, Pau France

(*Electronic mail: germain.vallverdu@univ-pau.fr)

(Dated: 25 September 2022)

This article presents a new reactive potential in the ReaxFF formalism. It aims to include the chlorine element, and opens up the fields of use of ReaxFF to the whole class of organochloride compounds including conjugated or aromatic groups. Numerous compounds in this family raise global awareness due to their environmental impact, and such a reactive potential will help investigate their degradation pathways. The new force field, named CHONCl-2022_weak, belongs to the aqueous branch. The force field parameters were fitted against high-level quantum chemistry calculations, including CASSCF/NEVPT2 calculations and density functional theory calculations, and its accuracy was evaluated using a validation set. The root means square deviation against quantum mechanics energies is 0.38 eV (8.91 kcal mol^{-1}). From a structural point of view, the root means square deviation is about 0.06Å for the bond lengths, 11.86° for the angles and 4.12° for the dihedral angles. With CHONCl-2022_weak new force field, we successfully investigated the regioselectivity for nucleophilic or electrophilic attacks on polychlorinated biphenyls (PCB), which are toxic and permanent pollutants. The rotation barriers along the bond linking the two benzene rings, which is crucial in the toxicity of these compounds, are well reproduced by CHONCl-2022_weak. Then our new reactive potential is used to investigate the chlorobenzene reactivity in the presence of hydroxyl radicals in atmospheric condition or in aqueous solution. The reaction pathways computed with ReaxFF agree with the quantum mechanics results. We showed that, in the presence of dioxygen molecules, in atmospheric condition, the oxidation of chlorobenzene likely leads to the formation of highly oxygenated compounds after the abstraction of hydrogen radicals. In water the addition of an hydroxyl radical leads to the formation of chlorophenol or phenol molecule, as already predicted from plasma-induced degradation experiments.

I. INTRODUCTION

Computational chemistry provides powerful methodologies in order to investigate chemical systems, including classical molecular mechanics approaches, the fastest and quantum mechanics (QM) methodologies, the most accurate. Considering the investigation of the chemical reactivity of complex systems, a methodology accurate enough to describe bonds breaking and formation is needed at an atomic resolution. Bridging the gap between molecular mechanics and a more sophisticated approach such as quantum chemistry, ReaxFF is a reactive potential based on the so-called bond order. It allows chemical reactions to be considered in molecular dynamics simulations of large systems. ReaxFF, developed since 2001 by van Duin *et al.* [1], has proven its efficiency in describing reactive systems of various domains and different phases, including a wide variety of elements[2]. It was initially designed to study organic compounds with carbon and hydrogen atoms to focus on combustion reactions[1]. However, it rapidly increased its field of application since the CHO reactive force field publication by Chenoweth *et al.* [3] in 2008. Many variations appear from this new force field, and a wide variety of force fields were published divided into two main branches called the aqueous branch and the combustion branch[2].

One of these force fields called Protein-2013, coming from the aqueous branch, was a step forward when it was published[4]. Indeed it allows for the first time to investigate the reactivity of biomolecules through molecular dynamics simulations, including water as a solvent. All the elements needed to consider amino acids were parameterized, including, in particular, nitrogen, sulfur and counter ions. This force field has been updated twice in 2017[5] and 2018[6] with a better description of the weak forces and has become the well-none force field CHON-2017_weak force field used in numerous works[7–9].

This new version of ReaxFF can be implemented to investigate the degradation pathways of organic molecules. One point of particular interest in the nowadays environmental context would be the ability to consider the chlorine element. Indeed, organochlorides are compounds widely used in the last half-century in an industrial or pharmaceutical context[10–12]. Because of their chemical stability, these organochlorides are measurable in different environments[13], such as soil[14], water[15], the atmosphere[16], living-organism[11] and food[17]. Among the organochlorides, organochloride pesticides and PCBs (polychloride biphenyls) raise global awareness due to their environmental impact and their hight toxicity[18,19]. The DDT (dichlorodiphenyltrichloroethane) and TCDD (2,3,7,8-Tétrachlorodibenzo-p-dioxin) are both organochloride pesticides with high toxicity and

persistence[20–22]. Even if they were identified as toxic, persistent compounds and prohibited since 2001 by the United Nations Environment Program[19], they are still used in some countries[10,13]. PCBs were highly produced with around 1,325,810 tons[23] since 1930 in different manufacturing products. Their worldwide presence was proven in all environments and capable of biomagnifying along the trophic chain[24,25]. It was identified that 12 of the 209 PCBs were particularly toxic with an important TEF (toxicity equivalent factor)[26] due to a low torsional angle between the two cycles allowing them to arrange their structures easily[27].

The investigation of these compounds' reactivity in different environments is of great interest to understand their degradation, which will allow the development of new treatment processes and a better understanding of the toxic effect on the environment and health. In the last decade, the reactivity of organochlorides and in particular the different enantiomers of the DDT, TCDD and PCBs, have been investigated through computational approach[28–34]. The degradation processes were investigated from molecular dynamics simulation on the DDT in a water-sediment environment, and several studies have implemented atmospheric reactions initiated by radicals such as OH, CH or molecules such as O_3 and H_2O_2.

ReaxFF parameters for the chlorine element were first provided in the Protein-2013 force field where chlorine was included as a counter ion[4]. It was also parameterized in two different force fields to deal with oxidative degradation of organic matter in geological formations[35] and explosive compounds[36]. In both cases, the parameter set is not transferable enough to consider organochloride compounds, particularly for conjugated or aromatic molecules.

In this work, we describe the parametrization of a new reactive force field, named CHONCl-2022_weak, based on the CHON-2017_weak force field. It aims to include the chlorine element, and opens up the fields of use of ReaxFF to the whole class of organochloride compounds including conjugated or aromatic groups. We decided to start from the CHON-2017_weak as it was the last version of a CHON reactive force field in the aqueous branch. After a quick review of the ReaxFF methodology, we describe the training set and the validation set implemented in this work and the computational details linked to reference calculations. The parameters are obtained against the QM calculations. The comparison with the validation set is detailed, considering bonds, angles and dihedrals internal degrees of freedom along with charge distribution and reaction pathways. The validation set includes PCB molecules. Then the reaction pathways of the chlorobenzene oxidation are investigated from QM calculations and ReaxFF simulations, including the regioselectivity of the reaction with the hydroxyl radical.

II. COMPUTATIONAL METHODS

A. A novel ReaxFF reactive potential

ReaxFF is a force field based on the bond order (BO), which makes that quantity the key point that tunes the various energy terms. The main consequence is that ReaxFF is able to describe bond dissociation and enable the investigation of large reactive systems[3]. The following equation represents the complete equation with all energy terms which contribute to the total energy:

$$E_{system} = E_{bond} + E_{lp} + E_{over} + E_{under} + E_{val} + E_{pen} + E_{coa} + E_{C2} + E_{triple} + E_{tors} + E_{conj} + E_{Hbond} + E_{vdW} + E_{Coulomb} \quad (1)$$

All these energetic terms are divided into two main groups: intramolecular interactions (11 terms) and intermolecular interactions (3 terms). The common factor in intramolecular interactions are their dependence upon the BO. Following the terms in equation (1), the intramolecular terms describe the bond, lone pair, overcoordination, undercoordination, valence angle, correction of double bonds angle valency issues, correction for NO_2 group stability, correction to destabilize triple bond for carbon, a particular correction for carbon monoxide, torsions and conjugation energies. On the other hand, the intermolecular interactions include the Van der Waals, Coulombic and hydrogen-bond interactions. More details are available in the literature, and we invite the reader to look at the article of Chenoweth *et al.* [3] for further information.

The CHON-2017_weak version was used as the initial force field by including the chlorine atoms and the associated bond, angle and torsion parameters. A total of 68 parameters have been parameterized including parameters associated to valence and non-bonded terms of the equation (1). Even for a single element, this represents a huge number of parameters to optimize, leading to a complex optimization procedure, particularly due to correlations between parameters. In the following, we give some hints by describing the steps we followed during this optimization.

As done in previous works[3], the required parameters are optimized against quantum mechanics (QM) reference calculations. The computational details associated with the different methods used to implement these calculations are presented in the following sections.

Primarily, a training set and a validation set were made. They include a set of molecules and small reaction pathways representing all the internal coordinates as bonds, angles, and torsions necessary to mimic the reactivity of organochloride. For example, the potential energy surface

(PES) of the bond dissociation of the C-Cl bond in the chlorobenzene, as well as the geometrical parameter of its optimized structure, were added to the training set for the C-Cl bond parametrization. The training set and the validation set files, including energy values and geometries of the compounds along PESs are given in the supplementary information.

The stochastic optimizer CMA-ES (Covariance Matrix Adaptation Evolution Strategy)[37], implemented in the REAX module of Amsterdam Modeling Suite (AMS)[38], was used to optimize the parameters. This algorithm considers the correlation between the parameters thanks to the implementation of covariance behaviour. Like all the evolutionary algorithms, CMA-ES is partly based on biological evolution and tends to obtain the optimal population iteratively by minimizing an error function, the fitness, defined as followed:

$$Fitness = \sum_{i=1}^{n} \left[\frac{x_{i,train} - x_{i,ReaxFF}}{\sigma_i} \right]^2 \tag{2}$$

where the differences between the reference values, $x_{i,ref}$ and the ReaxFF values, $x_{i,ReaxFF}$, are weighted by σ_i values. These σ_i weights are manually chosen depending on the accuracy of the reference or its utmost importance. For example, the weight of the accurate CASSCF calculations can be higher than that made with DFT. Moreover, it is necessary to consider the number of points in each PES in order to avoid overfitting this coordinate.

One crucial step before the CMA-ES optimization is to build an initial set of parameters and their individual boundaries. Thus, the parameter values were chosen by mimetism with the same parameters of a different element in the CHON-2017_weak force field or compared with the values of identical parameters in different force fields containing chlorine. For the first boundaries, broad limits were chosen. However, in order to manage the correlation between the parameters, the optimization was split with no more than 25 parameters optimized simultaneously, starting by optimizing C-Cl and Cl-H bond parameters with the angle and torsion parameters containing these bonds, then Cl-O and finally Cl-Cl.

It leads to a process of optimization of the parameters in three successive parts. Starting from the previous set of parameters, we proceed as follows in each part. Several cycles of hundreds of CMA-ES optimizations were produced with broad boundaries, leading to sets of one hundred optimized parameters. Then, from this set, we analyzed the distribution of each parameter in order to narrow the boundaries and avoid bimodal distributions. Moreover, we also investigated the distribution of all the different fitness obtained, which helps identify groups of force fields that are not well optimized. On the other hand, we analyzed the correlation between the parameters

in the population of optimized force fields. We used it as an indicator of well-defined boundaries for the parameters by reducing the correlation between them as much as possible. Considering the parameter distributions, the fitness distribution and the correlation analyzes, the parameter boundaries were manually improved in each cycle of CMA-ES optimization runs until we stabilize a set of parameters.

Finally, at the end of the three parts of the last parameters optimization, the new CHONCl-2022_weak force field was chosen according to the one with the lowest fitness and by comparison with the validation set. The file, including the parameters, is provided in the supporting information in the format suitable for LAMMPS[39].

B. Computational details, quantum chemistry methods

This part presents the computational details associated with the quantum chemistry methods implemented to build the training set and the validation set. These sets consist of PES, relative energies and geometrical data such as bond lengths, bending angles and dihedral angles.

One essential reference values associated with ReaxFF are the bond dissociation energies (BDE). In this work, we used complete active space self-consistent field (CASSCF) calculations[40] to compute the BDEs. Indeed, at the dissociation limit, the multireference character of the wave-function needs to implement such high level methodologies to gather accurate results.[41]. Details about the CASSCF calculations are presented in the supporting information in the table S1 with the selected active spaces associated. Moreover, NEVPT2[42] calculations, including a perturbation theory correction at the second-order were considered. The calculations were done with ORCA software version 4.2.1[43] and the cc-pVTZ basis set[44].

Density functional theory (DFT) calculations were made apart from the BDE calculations to obtain the PES along bending angles and dihedral angles. The calculations were driven with Gaussian 16[45], using the B3LYP functional[46–49], the 6-31+g(d) basis set[50–52] and the GD3BJ empirical dispersion model[53].

The training and validation sets include reaction pathway and transition states geometries obtained using an in-house Chain-of-States methodology[54] coupled to Gaussian 16 program. In order to keep the consistency with the PES calculations, the B3LYP functional with the 6-31+g(d) basis set and GD3BJ empirical dispersion were used. After the Chain-of-States process, the transition state geometry was optimized. The frequencies were computed, and we verified the presence of

one single imaginary frequency. Moreover, using the same methodology, we computed transition states energies using the M06-2X DFT functional and the basis set 6-311++g(2df,2p) for further comparison with available results in the literature.

Bond lengths were computed at the MP2[55–59] level with the cc-pVTZ basis set using the ORCA software version 4.2.1[43]. This calculation level is well known for its accuracy in reproducing this geometrical data.

C. Molecular mechanics and molecular dynamics

All the calculations at the ReaxFF level were done using either the Large-scale Atomic/Molecular Massively Parallel Simulator[39] code (LAMMPS) version October2021, or the REAX module of the AMS software[38]. For the comparison of BDE, all PES along internal coordinates and reaction pathways, the ReaxFF energies were computed on the geometries obtained at the QM level of calculations included in the training set or the validation set. Defaults LAMMPS cutoff parameters were used in all ReaxFF calculations, in particular nbrhood_cutoff equal to 5Å and hbond_cutoff equal to 7.5Å.

Considering molecular dynamics simulations in water or in atmospheric condition a timestep of 0.1 fs was used for all the simulations, in the NVT ensemble using the Nose-Hoover thermostat[60,61]. In the atmospheric investigation, constant temperature simulations were implemented, whereas, in the water degradation, we used a ramp of temperature between 550 K and 750 K over a simulation time of 2 ns.

III. RESULTS AND DISCUSSIONS

A. Force field validation against QM calculations

The new CHONCl-2022_weak force field was validated by comparing the ReaxFF energies with energies obtained from high-level quantum chemistry calculations at the CASSCF/NEVPT2 level or calculations at the B3LYP/6-31+g(d) level. The root mean square deviations (RMSD) of the energy differences are 8.36 kcal mol^{-1} (0.36 eV) and 8.91 kcal mol^{-1} (0.39 eV in the training set and the validation set, respectively. For comparison, Hur *et al.*[35] obtained a RMSD of the energy of about 1.57 eV for their force field optimized to investigate the degradation of compounds with oxychlorine.

Considering references to molecular structures, the RMSD on bond lengths is about 0.06 Å and considering bending angles and dihedral torsions, the RMSD are 11.86° and 4.12° respectively. The RMSD obtained on angles is surprisingly much higher than the one on torsion. This is mainly due to the Cl-C-H angle in chloroethane and chloroethanol. Indeed, this angle is highly overestimated by the CHONCl-2022_weak force field and represents more than 30% of the total error between the QM values against the ReaxFF ones.

1. Bond dissociation energy and bond lengths

This section compares the PES and BDE energies computed at the CASSCF/NEVPT2 level to ReaxFF results. In the figure 1, there are the four PES along the different bonds parametrized in the new force field. The PES of the dichloride (Cl_2) and the acetyl chloride (CH_3OCl) molecules belong to the training set, while the chloromethanol (CHOHCl) and the hydrogen-chloride (HCl) molecules belong to the validation set. From a general point of view, the ReaxFF PES follow with acceptable accuracy the QM PES for the four molecules. Some differences appear at large distances. For chloroethane and chloroethanol, differences appear above 2.6Å, as the results obtained by Hur *et al.* [35]. This can be explained by the overestimation of the Cl-C-H angle. For the dichloride molecule, the ReaxFF PES seems to reach a plateau for distances larger than 3Å. This is due to the values of the BO that vanish at this distance, and thus only non-bonded interactions remain for such distance.

The BDE values are gathered in the table I. CHONCl-2022_weak's BDE complies with the BDE computed at the CASSCF/NEVPT2 level, both in the training and the validations set, even if the BDE tend to be slightly underestimated. For the C-Cl bond in chlorobenzene, chloromethane and chloromethanol, BDE differences between QM and ReaxFF are less than 0.15 eV. For the Cl-Cl bond, the difference is around 0.24 eV, and for the Cl-O bond, the difference is equal to 0.26 eV, which are acceptable values comparing other ReaxFF force fields in the literature. Concerning the C-Cl bond in chloroethane and chloroethanol, the differences in the BDE are 1.14 and 1.49 eV, respectively, which is larger than the RMSD. In H-Cl, the BDE is 0.68 eV which is also larger than the RMSD. Nevertheless, these differences are still lower than the energy RMSD of 1.57 eV of Hur *et al.* [35] and still acceptable.

Then we focus on the molecular geometry and compare the bond lengths obtained with ReaxFF and those obtained at several QM levels. The bond lengths are reported in the table II. The bond

Molecule	Bond	CASSCF/NEVPT2	ReaxFF	set
Dichlore	Cl-Cl	2.81	2.57	T
Chlorobenzene	C-Cl	4.23	4.19	T
Chloromethane	C-Cl	3.48	3.33	T
Chloromethanol	C-Cl	3.56	3.44	V
Chloroethan	C-Cl	3.63	2.18	V
Chloroethanol	C-Cl	3.85	2.36	V
Methyl hypochlorite	O-Cl	1.92	1.66	T
Hydrogen chloride	H-Cl	4.63	3.95	V

TABLE I. Bond dissociation energies (in eV) associated with the parameterized bonds in the considered molecule at the QM CASSCF/NEVPT2 level and the ReaxFF CHONCl-2022_weak level. The last column indicates if the corresponding bond is in the training set (T) or the validation set (V).

lengths obtained with CHONCl-2022_weak well reproduced the QM values for bonds both in the training set and the validation set with a slight overestimation. The largest deviation is observed for the chloroethanol with 0.1Å.

CHONCl-2022_weak overestimates the Cl-Cl bond distance with a maximum error of 0.2 Å. Here, we reached the limitation of the optimization starting from a previous force field. Indeed, we could have improved the distances between the chlorine atom, but it has considerable repercussions. For example, shortening the Cl-Cl bond distance leads to high difficulties in reproducing the density of different chloride solvents. CHONCl-2022_weak reproduces well the densities of common chlorinated solvents, see table S2 in the supporting information. It also makes aromatic molecules with two chlorine atoms in ortho positions unstable, for example, in PCB structures. This small error on the Cl-Cl bond is thus a compromise and is still tolerable.

2. PES along bending angles

Here PESs at the B3LYP/6-31+g(d) level of several bending angles are considered and compared to the one computed with CHONCl-2022_weak, see figure 2. From a general point of view ReaxFF PESs agree well with the DFT results. Concerning the Cl-C-C angle of the chloroethane, as in the case of BDE, it is responsible for the largest contribution of the RMSD for bending angle

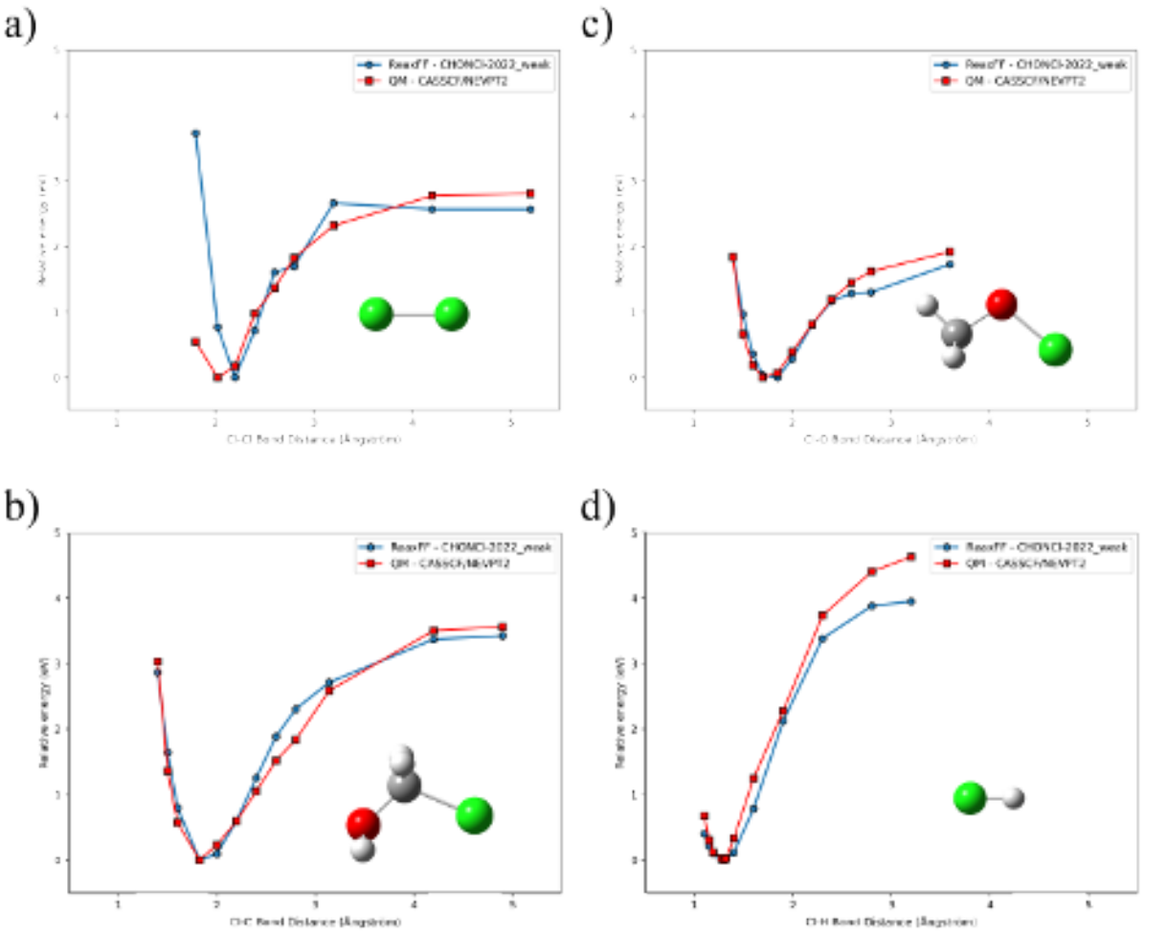

FIG. 1. Comparison between PES (in eV) along bond dissociations obtained with ReaxFF (blue circle) and at the QM CASSCF/NEVPT2 level (red square) as a function of the bond distance (in Å). a) Cl-Cl bond in dichloride molecule; b) Cl-C bond in chloromethanol; c) Cl-O bond in acetyl chloride and d) Cl-H bond in hydrogen chloride. The molecules are depicted on the different graphics with the chlorine atom in green, carbon in grey, hydrogen in white and oxygen in red.

, which is 11.86°. In a non-conjugated system, the force field tends to overestimate the repulsion induced by the chlorine atom, leading to a shift of the PES of this bending angle. However, the difference coming from the table III is about 19°, which is still acceptable for the force field.

From the table III, there is a good agreement between the angles obtained on the full optimized structure at the B3LYP/6-31+g(d) level and with CHONCl-2022_weak. Nevertheless, the C-C-Cl bending angle of the PCB101 with a chlorine atom in the ortho position is also overestimated

		QM				
Molecule	Bond	CASSCF	B3LYP	MP2	ReaxFF	set
Dichlore	Cl-Cl	2.02	2.05	2.00	2.20	T
Chlorobenzene	C-Cl	1.77	1.76	1.74	1.74	T
Chloromethane	C-Cl	1.81	1.81	1.78	1.82	T
Chloromethanol	C-Cl	1.83	1.84	1.80	1.87	V
Chloroethan	C-Cl	1.83	1.82	1.79	1.85	V
Chloroethanol	C-Cl	1.82	1.81	1.78	1.88	V
Methyl hypochlorite	O-Cl	1.71	1.73	1.69	1.81	T
Hydrogen chloride	H-Cl	1.27	1.29	1.27	1.29	V

TABLE II. Comparison of the bond lengths obtained at several QM levels (CASSCF/NEVPT2, DFT, MP2) and the CHONCl-2022_weak force field. The last column indicates if the corresponding bond is in the training set (T) or the validation set (V).

Molecule	Angle	B3LYP	ReaxFF	set
PCB101	C-C-Cl (ortho)	120.2	137.8	V
PCB101	C-C-Cl (meta)	117.2	118.9	V
Chlorobenzene	C-C-Cl	119.3	121.5	V
Chloromethane	Cl-C-H	108.6	105.6	V
di-Chlorobenzene-ortho	C-C-Cl	118.8	118.7	V
Chloroethan	C-C-Cl	111.4	130.6	V
Methyl hypochlorite	C-O-Cl	110.4	119.3	V

TABLE III. Comparison of the angle (in degrees) obtained at the B3LYP/6-31+g(d)/D3BJ level and the CHONCl-2022_weak force field. The last column indicates if the corresponding angle is in the training set (T) or the validation set (V).

at around 17°. This difference is due to the dihedral angle around the central bond between the two cycles, which is small in the case of CHONCl-2022_weak. This leads to higher repulsion between the chlorine atom with the opposite hydrogen in the ortho position. However, when the two aromatic cycles of the PCB101 become more tilted, this bending angle rapidly decreases

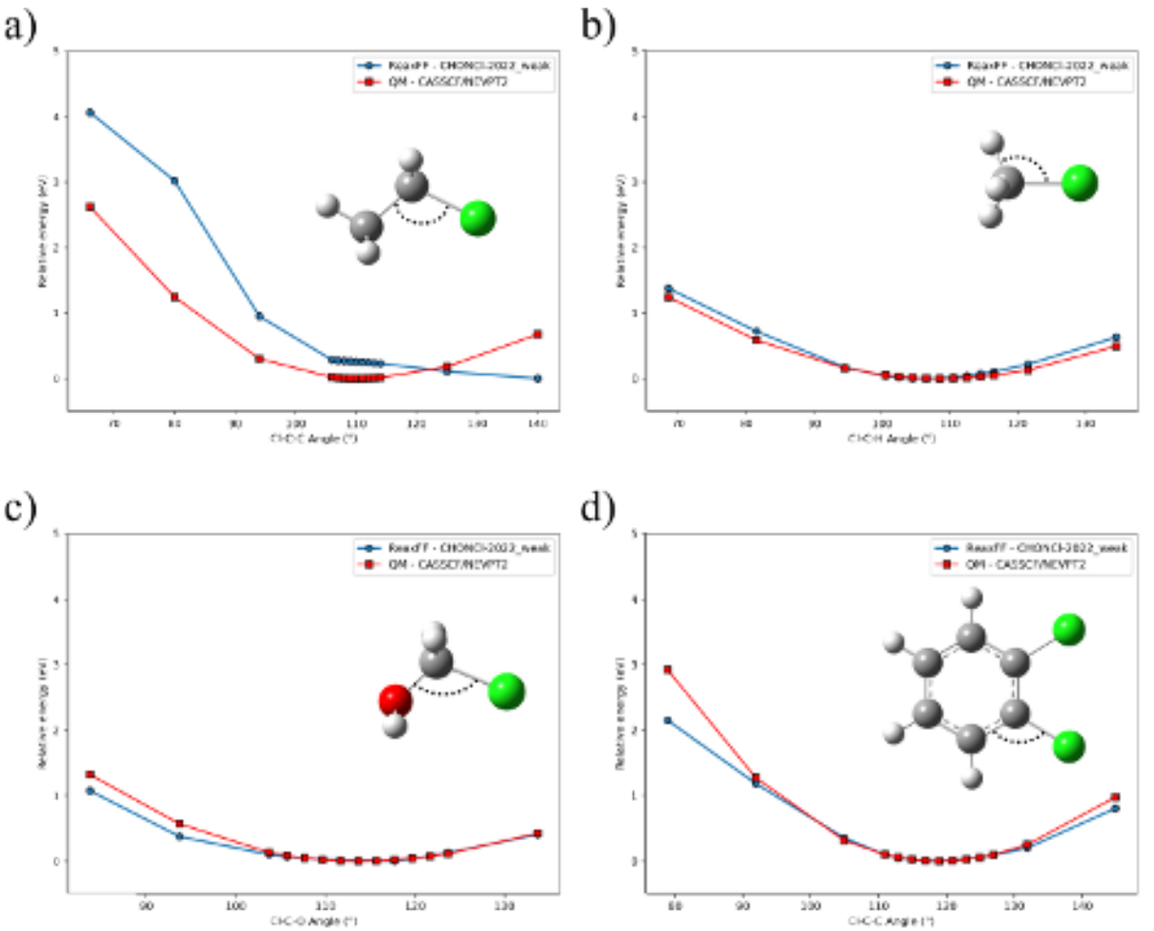

FIG. 2. ReaxFF (blue circle) and QM-B3LYP/6-31+g(d)/D3BJ (red square) comparison of the relative energy (eV) as a function of the angle (in degrees) for the Cl-C-C angle of the chloroethane, the Cl-C-H of the chloromethane, the Cl-C-O of chloromethanol and the Cl-C-C of the ortho-dichlorobenzene. There is a representation of these molecules on the different graphics with the chlorine atom in green, carbon in grey, hydrogen in white and oxygen in red. Black dotted points show the angle concerned by the PES.

around 120°, similar to the QM value.

3. PES along dihedral angles

This section compares the PESs of torsions along dihedral angles obtained at the B3LYP/6-31+g(d)/D3BJ level against the CHONCl-2022_weak values. In the case of PCBs, the torsion around the biphenyl central bond is of high interest as it plays a significant role in their toxicity[27].

Molecule	dihedral	QM	ReaxFF	Set
p-dichlorobenzene	Cl-C-C-H	360.0	360.0	V
Chlorobenzene	Cl-C-C-C	180.0	180.0	V
Chloromethanol	Cl-C-O-H	67.4	68.6	V
Chloroethanol	Cl-C-C-O	179.7	180.0	V
Methyl hypochlorite	H-C-O-Cl	180.0	180.0	V
Chloroethan	Cl-C-C-H	299.6	299.6	V
o-dichlorobenzene	Cl-C-C-Cl	360.0	360.0	V
PCB101	Cl(para)-C-C-C	179.9	183.2	V
PCB169	Cl-C-C-Cl	359.5	359.9	V

TABLE IV. Comparison of the dihedral angle (in degrees) obtained at the QM-B3LYP/6-31+g(d)/D3BJ level and the CHONCl-2022_weak force field. The last column indicates if the corresponding dihedral angle is in the training set (T) or the validation set (V).

The value of this central torsion for different PCBs, as well as some activation barriers are included in the validation. The PCBs considered in this work are depicted in figure S1 in the supporting information. PES along four dihedral angles are depicted in figure 3. The PES of the chloromethanol and PCB101 were in the training set, while the p-dichlorobenzene and the PCB169 were in the validation set.

For the dichlorobenzene and the chloromethanol, CHONCl-2022_weak reproduces almost identically the QM PES along the Cl-C-C-H and the Cl-C-O-H angles. At the same time, small differences are obtained between the two PCBs. For the PCB101, ReaxFF reproduces well the repulsion between the chlorine and hydrogen atoms when the C-C-C-C torsion is equal to 0° and 360°. The position of the minimum is shifted between QM and ReaxFF PES, but it belongs to a flat part of the PES and is acceptable. Concerning the PCB169, the PES is slightly overestimated when it has a planar structure at 0° and 360° and a little underestimated when the two cycles are perpendicular, 90°. Such deviation can be improved by using the torsions 2013 version available in the AMS Software[38] and the tapered bond orders of Furman and Wales[62], see table V.

Table IV presents the values of several kinds of dihedrals angles that were considered in the validation set. The values obtained with CHONCl-2022_weak are in good agreement with the QM ones and present a deviation lower than the global RMSD over dihedral angles of 4.12°.

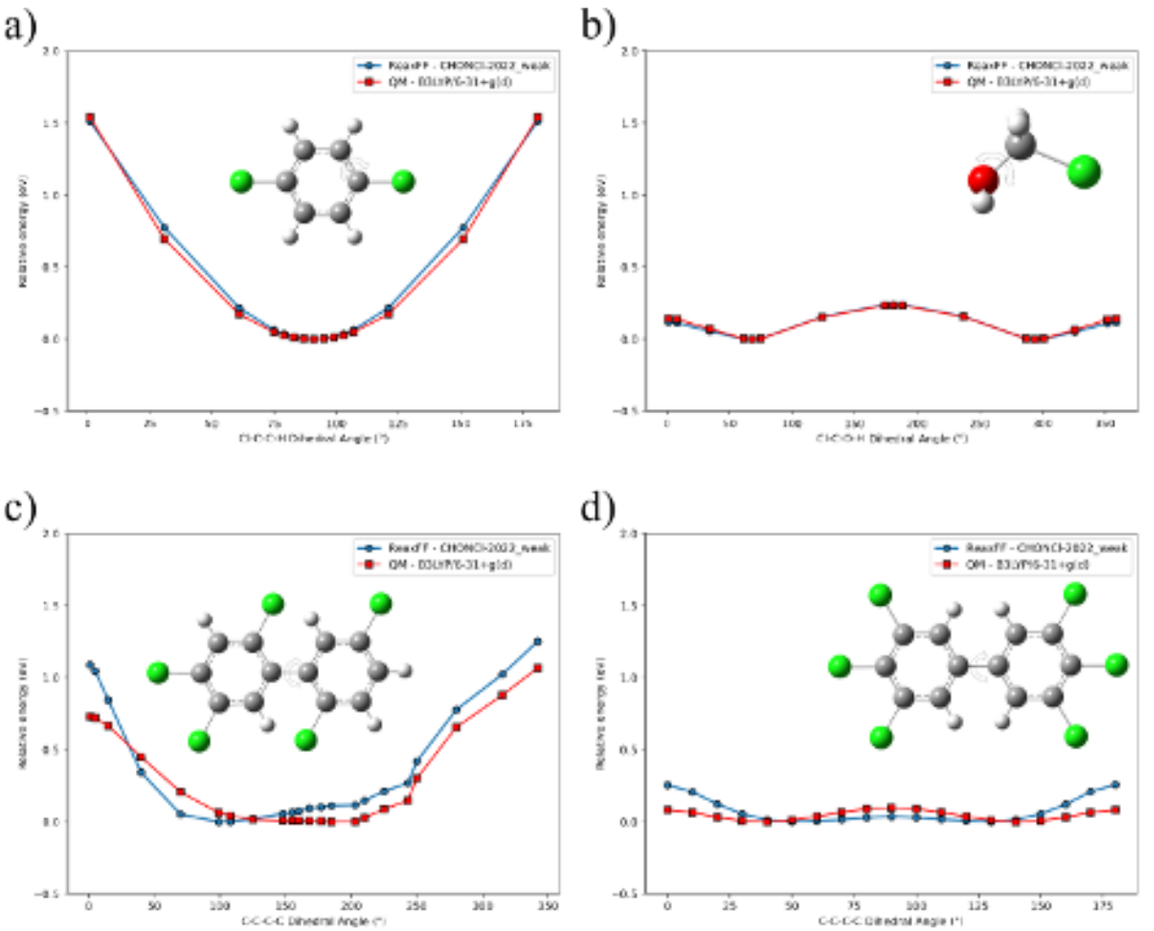

FIG. 3. CHONCl-2022_weak ReaxFF (blue circle) and QM-B3LYP/6-31+g(d)/D3BJ (red square) PES (in eV) along several dihedral angles (in degrees). a) the Cl-C-C-H torsion of the p-dichlorobenzene, b) the Cl-C-O-H of the chloromethanol, c) the C-C-C-C torsion around the central bond of the PCB101 and the PCB169 (d). There is a representation of these molecules on the different graphics with the chlorine atom in green, carbon in grey, hydrogen in white and oxygen in red. Black arrows indicate the considered dihedral angle.

The rotational barrier of several PCBs was then considered to discuss the validity of the CHONCl-2022_weak force field. Hereafter the rotational energy barriers and the optimized values of the dihedral angle between the two phenyl rings are considered. Two quantities were computed: ΔE^0 is the energy barrier to reach a planar conformation from the optimized geometry, and ΔE^{90} is the energy barrier needed to reach a perpendicular conformation, with an angle of 90°

between the two phenyl rings, from the optimized geometry. The values obtained with CHONCl-2022_weak are compared to those available in the literature or computed at several QM levels of calculation, see table V. In 1981, McKinney and Singh[63] explained that the PCBs considered as toxic, have at least four laterals chlorine atoms. The PCBs with the lowest rotational energy barrier are more flexible, leading to better associations with bio-molecules and increasing their toxicity[27]. These rotational barriers are strongly impacted by the presence of chlorine atoms in ortho positions, which increases the needed energy to reach the planar conformation. In consequence, PCBs 126 and 169 presented in the SI figure S2 are among the more toxic and present only one or no chlorine atom in the ortho position.

Looking at table V, the dihedral angle values of the torsion between the two phenyl rings are well reproduced as well as the relative values between PCBs, the largest error being a deviation of 5° for PCB77 with the closest reference value. These results enforce the validity of the Van der Waals parameters optimized for the chlorine atom which mainly drive the equilibrium values along this torsional motion. Globally, CHONCl-2022_weak tends to underestimate the values slightly. The same conclusion can be drawn considering the energy barriers. CHONCl-2022_weak reproduces well the significant increase of the energy barrier ΔE^0 in the case of the presence of chlorine atoms in ortho positions. For example, one can consider the comparison of ΔE^0 and ΔE^{90} in the case of PCB101 and PCB52 both wearing chlorine atoms in ortho positions. On the contrary, the PCBs that do not have ortho chlorine atoms have a low rotational barrier leading to high flexibility. For example, for the most toxic PCBs 126 and 169, energy barriers are in agreement with reference values provided in table V and literature investigations of these PCBs assuming their flexibility.

4. Charge distribution

In figure 4 we focus on the carbon charge distributions of PCBs 52, 101 and 22. Literature values obtained with the Mulliken approximation from DFT calculations[66] are compared against ReaxFF ones using CHONCl-2022_weak to determine potential centres of nucleophilic and electrophilic additions. The variations of the charges are consistent over the carbon atoms when comparing the two levels of calculation. For the PCB22, presented in the figure 4 a), ReaxFF and DFT show a large positive charge on the carbon atoms 2, 3 and 4', which might be considered the most favourable nucleophilic sites. Moreover, the carbon 5,6 and 6' for ReaxFF and DFT show

a negative charge leading to a most favourable zone for electrophilic additions. Continuing this comparison for the PCB 52 in the figure 4 b), the carbon atoms 2 and 2' show the highest positive values for both methods, leading to the most favourable nucleophilic sites. Finally, for the PCB 101 figure 4 c), carbon atoms 4 and 5 exhibit the two highest positive charges for the two methods.

5. Validation against reaction pathways

Finally, we considered reaction pathways of small chlorinated molecules to compare the ReaxFF energies obtained with CHONCl-2022_weak with QM energies. Figure 5 displays four reaction pathways obtained at the B3LYP/6-31+G(d)/D3BJ level using a chain of state approach: a) the reaction between chloromethane and dihydrogen $CH_3Cl + H_2 \longrightarrow CH_4 + HCl$; b) the reaction between hydrogen-chloride and formic acid $HCOOH + HCl \longrightarrow HCOCl + H_2O$; c) the recombination of the HOCl molecule in HClO and d) the dissociation of chloromethanol in formaldehyde and hydrogen-chloride $CH_2Cl-OH \longrightarrow H_2CO + HCl$. The energy barriers obtained using the CHONCl-2022_weak force field are in the same order of magnitude as those obtained at the QM level, the largest error being 0.54 eV for the dissociation of chloromethanol. Moreover, it shows similar energetic differences between reactants and products with the maximum deviation of 0.57 eV.

In the case of the acid-base reaction presented in figure 5 b), ReaxFF underestimate the energy barrier of the reaction and the energy of the products. The gap overestimation between the transition state and the product might be due to the BO calculations in the case of acyl chloride systems with a carbon atom bearing both a chlorine atom and a C-O double bond. Indeed, the BO of C-Cl being lower than the BO of the C-O bond, the BO of the C-Cl bond is weakened at the expense of the BO of the C-O double bond. However, the difference between the QM energies and ReaxFF is about 0.57 eV and is still tolerable.

	Dihedral angles (degrees)		
PCBs	QM	ReaxFF	Exp.
PCB15	39.3[b], 37.9[e]	33.0	45.1 ± 1.5[a]
PCB52	95.5[c], 87.3[d], 81.3[e]	76.8	
PCB77	38.7[c], 37.7[e]	32.7	
PCB101	99.1[c], 77.2[d], 81.0[e]	92.4	
PCB126	39.2[c], 37.9[e]	37.7	
PCB169	38.9[c], 37.9[e]	43.1	

	Energy barriers (in eV)			
	ΔE^0		ΔE^{90}	
PCBs	QM	ReaxFF	QM	ReaxFF
PCB15	0.12[b], 0.09[a], 0.09[e]	0.04	0.11[b], 0.09[a], 0.11[e]	0.09
PCB52	0.72[c], 1.24[e]	1.55	0.003[c], 0.001[e]	0.04
PCB77	0.08[c], 0.08[e]	0.05	0.09[c], 0.11[e]	0.11
PCB101	0.69[c], 1.23[e]	0.49	0.002[c], 0.001[e]	0.06
PCB126	0.08[c], 0.08[e]	0.04	0.09[c], 0.11[e]	0.08
PCB169	0.07[c], 0.08[e]	0.08	0.09[c], 0.11[e]	0.08

TABLE V. Dihedral angles (in degrees) of the central C-C-C-C torsion along the biphenyl bond at equilibrium geometries from the literature or B3LYP/6-31+g(d)/D3BJ calculation level. The energy barrier of the rotation around the biphenyl bond (in eV) between the equilibrium geometry and the planar geometry, ΔE^0, or the perpendicular geometry ΔE^{90}. The values in the ReaxFF columns are obtained with the CHONCl-2022_weak force field.

[a]: Experimental value of Bastiansen and Samdal[64] ; [b]: this work B3LYP/6-31+g(d)/D3BJ ; [c]: Arulmozhiraja and Fujii[65] ; [d]: Gorbunova *et al.*[66]; [e]: Dorofeeva *et al.*[67], or with the new reactive force field. Rotational barrier ΔE^0 (planar structure) and ΔE^{90} (vertical structure) from QM are also compared with the ReaxFF values (in eV).

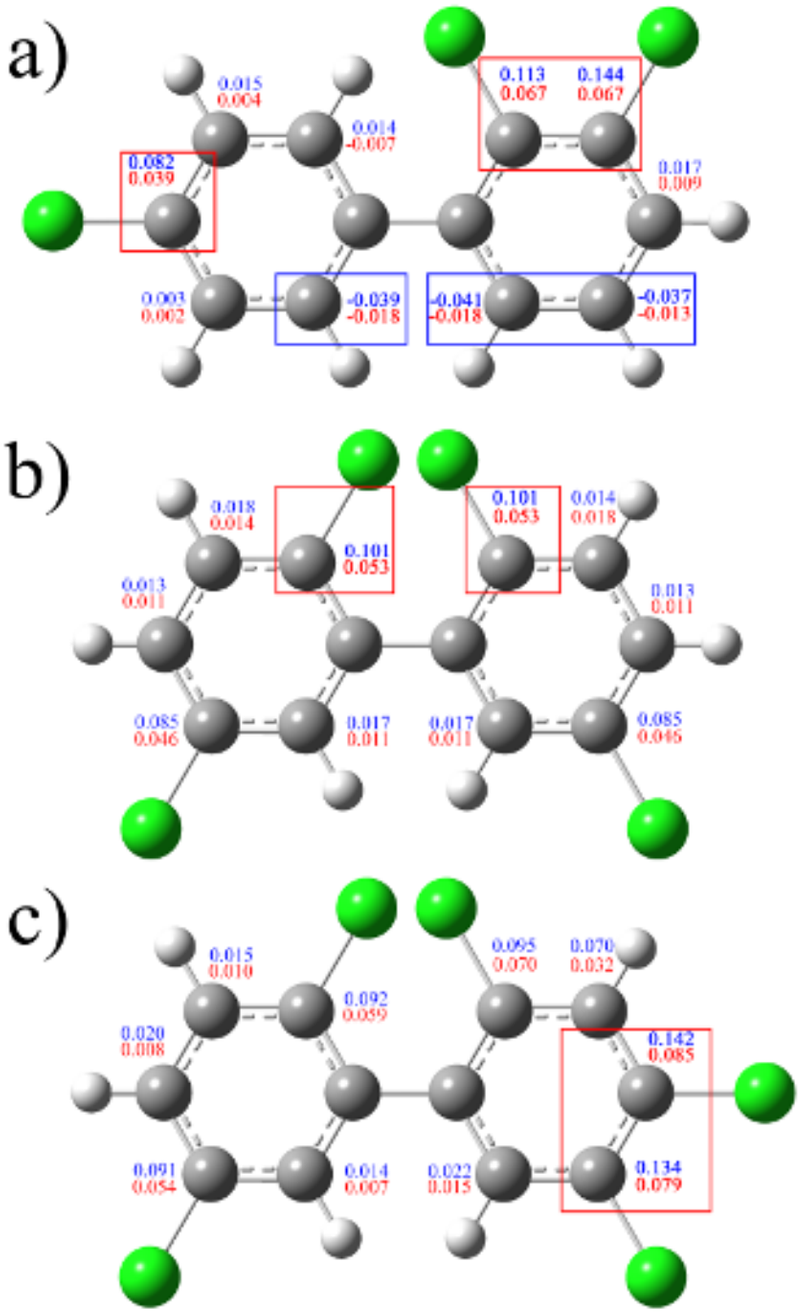

FIG. 4. Carbon atomic charges of several PCBs, a) PCB 22, b) PCB 52, and c) PCB 101, computed with ReaxFF CHONCl-weak_2022 (in blue) and DFT from the reference 66 (in red). Blue rectangles indicate the favourable carbon atoms for electrophilic additions and in red for nucleophilic.

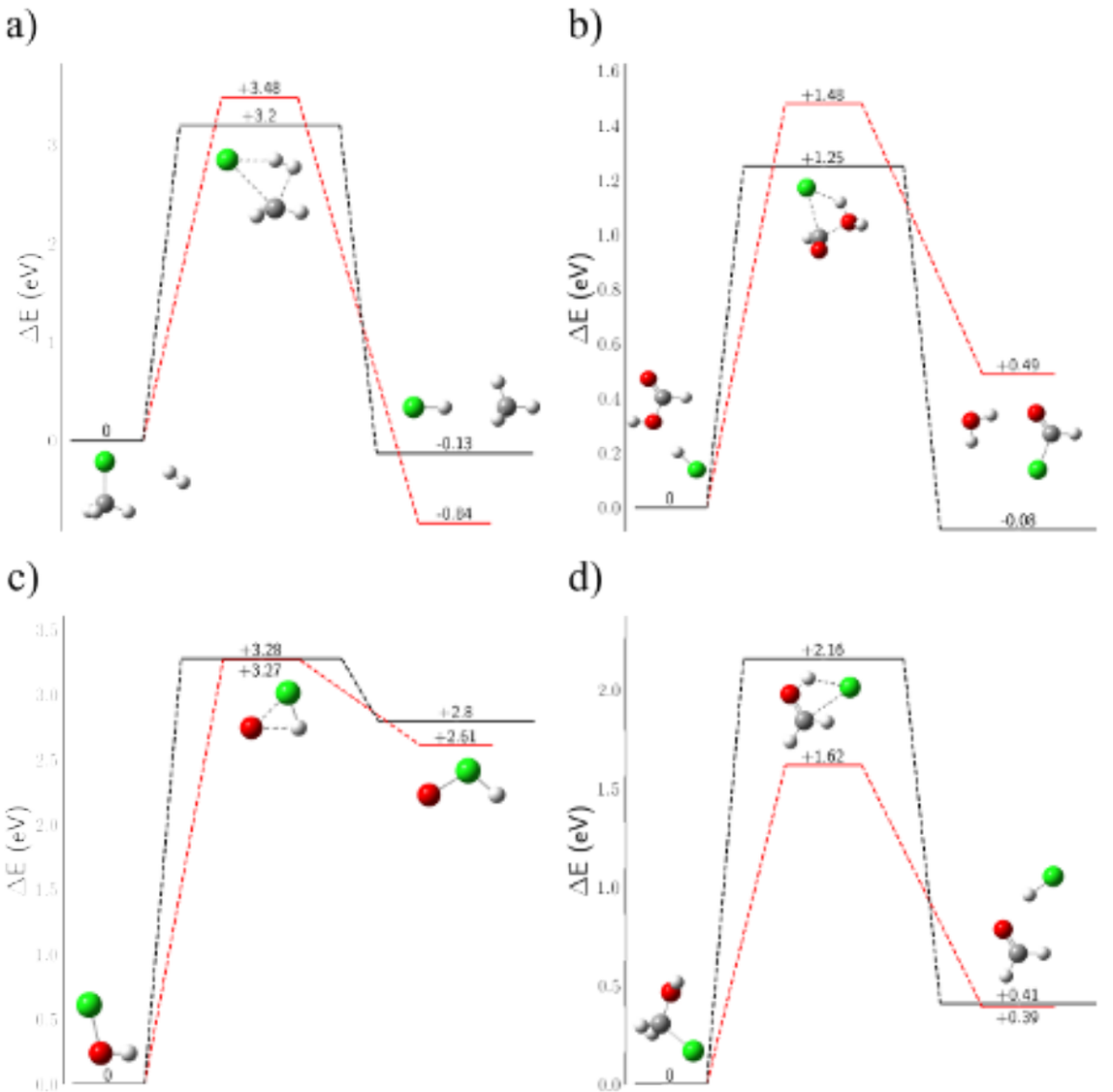

FIG. 5. Reaction pathways obtained at the B3LYP/6-31+g(d)/D3BJ level (red) and with CHONCl-2022_weak on the QM geometries (black) for the reactions a) $CH_3Cl + H_2 \longrightarrow CH_4 + HCl$, b) $HCOOH + HCl \longrightarrow HCOCl + H_2O$, c) the recombination of HOCl in HClO and d) the dissociation $CH_2Cl-OH \longrightarrow H_2CO + HCl$. There is a representation of these molecules on the different diagrams with the chlorine atom in green, carbon in grey, hydrogen in white and oxygen in red.

B. Atmospheric oxidation of chlorobenzene

In order to evaluate the performance of the new CHONCl-2022_weak force field, the oxidation of chlorobenzene initiated by hydroxyl radical is investigated. This section is divided into two parts. Firstly, reactive pathways of chlorobenzene obtained at the M062X/6-311++G(2df,2p) in relation to the work of Wu, Wang, and Wang[68] are compared with ReaxFF calculations with the new CHONCl-2022_weak force field. Kinetic and thermodynamics products are identified. Secondly, the regioselectivity of the hydroxyl radical oxidation process on the chlorobenzene is investigated, and the results are compared with the kinetic results of Bryukov *et al.*[69].

1. Investigation of the reactive pathway of chlorobenzene oxidation by hydroxyl radical in the presence of dioxygen

In this part, we consider the reactivity of chlorobenzene at the M062X/6-311++G(2df,2p) calculation level, consistently with the work of Wu, Wang, and Wang[68]) and using ReaxFF calculations with the CHONCl-2022_weak force field. The atmospheric gas-phase oxidation of the chlorobenzene initiated by hydroxyl radicals is investigated and presented in the figure 6. In the figure 6 a), the diagram corresponds to the reaction between the hydroxyl radical and the chlorobenzene in the ipso position corresponding to the carbon linked to the chlorine atom. Panel b), c), and d) correspond to the reaction between the hydroxyl radical and the chlorobenzene in ortho, meta and para positions, respectively, followed by the addition of dioxygen. For each of the different reaction pathways, the initial point, in the middle of each scheme, is the chlorobenzene with a hydroxyl radical. ReaxFF energies were computed using the QM optimized geometries. Two pathways were investigated by considering either the abstraction of a hydrogen atom leading to the formation of H_2O (the right side of each diagram of figure 6); or the addition of the hydroxyl radical on the aromatic rings (the left side of each diagram of figure 6). The only exception is the ipso reaction, where the right side of the diagram corresponds to the substitution of the chlorine atom by the hydroxyl radical. For ortho, meta and para reaction pathways, after both the addition or the H-abstraction, an addition of an O_2 molecule is then implemented to obtain final products, usually named highly oxygenated organic molecules (HOM) or chlorophenols. The energy barriers are in electron-volt and relative to the initial reactants except for the last products. After adding a dioxygen molecule, the barriers are relative to the previous states. QM calculations associated

with the hydroxyl radical addition (left side), were reported from the work of Wu, Wang, and Wang [68]. Globally CHONCl-2022_weak reproduces well the relative values of the QM energies of the reactive pathways but tends to overestimate the energy barriers of the reactions with the radicals.

Concerning the reaction of the OH radical in the ipso position (figure 6 a), the addition exhibit the largest energy barriers of all the reactive pathways, with both ReaxFF (1.12 eV and 1.02 eV) and QM levels of calculations (0.24 eV and 0.24 eV). These results agree with the conclusion of Wu, Wang, and Wang [68] and Bryukov *et al.* [69] that the ipso addition is, at ambient temperature, the least favoured reactive pathway. Moreover, the energy barrier of the reaction of the chlorine atom substitution (right side) is also a non-favoured pathway.

For the reactions in positions ortho, meta and para, figure 6 b, c and d, respectively, ReaxFF calculations reproduce the trends obtained at the QM level of calculation. The first tendency that we can notice, without considering the presence of dioxygen, is that both ReaxFF and QM calculations show that the addition of OH on the chlorobenzene (left side) is thermodynamically favoured. Indeed, in the three cases, the energies of products are lower than the energies of the products obtained after the hydrogen abstractions. However, we can observe a difference in the kinetic products obtained from ReaxFF and QM calculations. Considering the energy barriers, differences might be explained by the π-stacking arrangement of the hydroxyl radical above the benzene ring in the transition states geometries obtained from QM calculations which are not well described with ReaxFF due to the CHO parametrization. However, one specificity of these pathways is that the energy barriers on the two sides are closed to each other with differences at most about 0.1 eV in the range of the accuracy of the methodology. Our new ReaxFF potential well reproduces this point; thus, from a kinetic point of view, it is difficult to conclude on the most favoured pathway.

Now, if we consider the presence of the dioxygen molecule, we observe a good agreement between ReaxFF and QM calculations on products' energies and energy barriers. On the left side, after OH addition, the final products are the chlorophenol molecule in ortho, meta or para positions and the HO_2 molecule as suggested by Wu, Wang, and Wang [68]. On the right side, both QM and ReaxFF calculation levels do not present energy barriers from the products of the hydrogen abstraction to the formation of HOM with a dioxygen molecule crafted on the chlorobenzene ring. In the presence of dioxygen, ReaxFF with the new CHONCl-2022_weak force field predict that the formation of these HOM compounds are thus likely to happen[70]. These results complete the

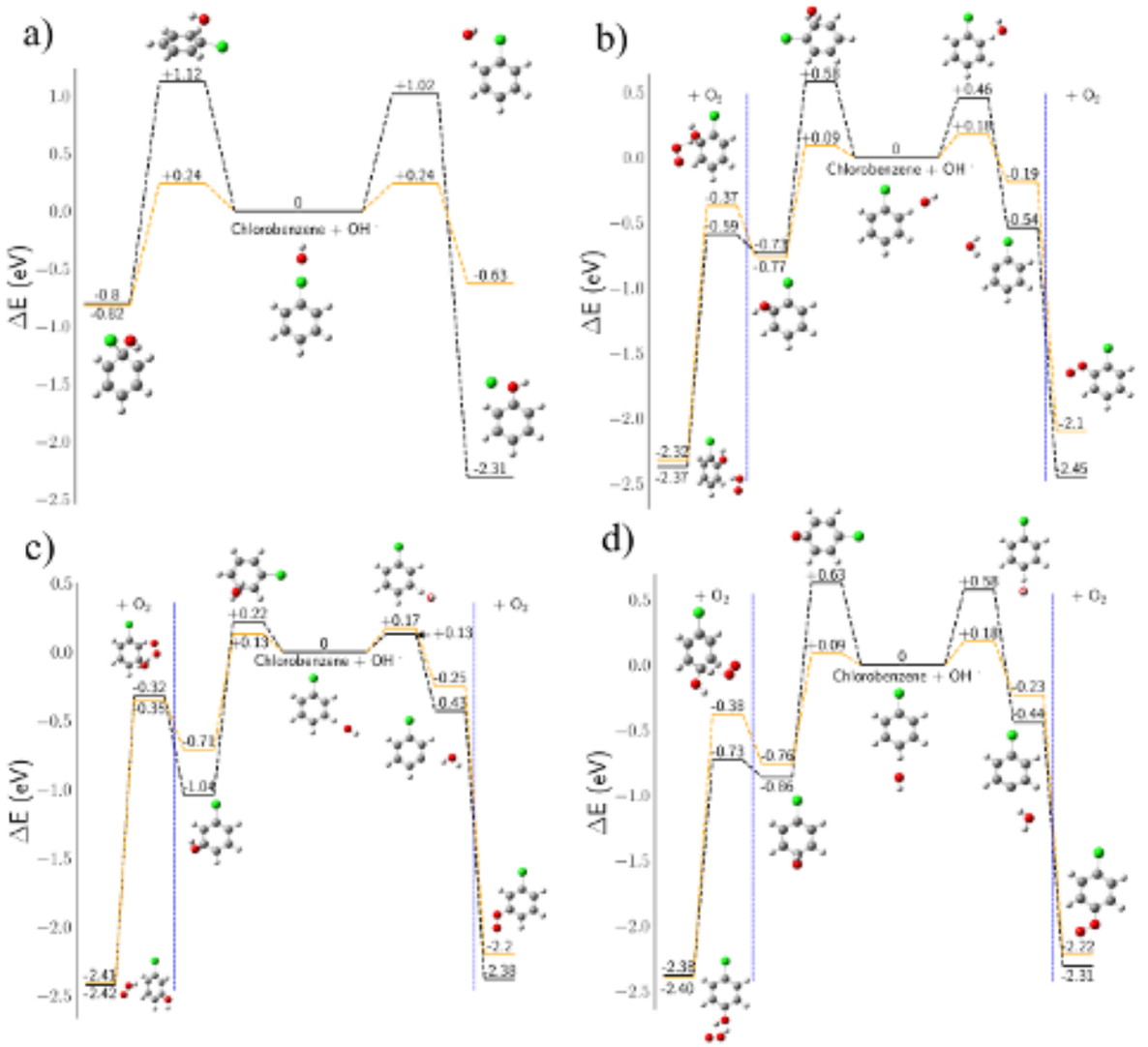

FIG. 6. Reaction pathways obtained at the M06-2X/6-311++g(2df,2p) level (orange from reference 68 or this work) and using ReaxFF with CHONCl-2022_weak (black). For all schemes, the initial reactants are chlorobenzene and hydroxyl radical in the middle. The left side corresponds to the addition of the hydroxyl radical, while the right side corresponds to the abstraction of a hydrogen atom of the phenyl ring. The reaction is done on the substituent in position a) ipso, b) ortho, c) meta and d) para. The final products are obtained after the reaction with dioxygen. The energy barriers are in electron-volt and relative to the initial reactants except for the last products, after the addition of dioxygen materialized by the blue vertical dashed lines, where in these cases, the barrier is relative to the previous state. There is a representation of all the different molecules on the different diagrams with the chlorine atom in green, carbon in grey, hydrogen in white and oxygen in red.

previous work of Wu, Wang, and Wang[68] on the chlorobenzene oxydation.

2. Regioselectivity of the chlorobenzene oxidation

Bryukov *et al.*[69] investigated the kinetics of the OH additions and the hydrogen abstractions on the chlorobenzene molecule from a combination of experimental and computational approaches. They agree with the QM conclusion of Wu, Wang, and Wang[68] by assuming that the primary reaction occurring at low temperatures are the OH addition and they showed that a shift appears around 450K, the hydrogen abstraction is becoming prominent. Moreover, they supposed that the hydrogen abstraction might occur at a lower temperature. To compare the values obtained by Bryukov *et al.*[69] with ReaxFF, the oxidation of the chlorobenzene molecule was investigated through reactive molecular dynamics simulations using the CHONCl-2022_weak force field.

In order to simulate atmospheric collisions, the chlorobenzene molecule was subjected to hydroxyl radical collisions coming from random positions sampled on a sphere centred on the centre of mass of the molecule. The initial velocity of the hydroxyl radical is oriented toward the centre of mass of the chlorobenzene molecule, and the velocity norm is sampled around the considered temperature. Then 8000 NVE simulations of 3 ps lengths were implemented to gather enough statistics using initial velocities at 80K, 250K, 300K, 350K and 800K. Most of the trajectories were inefficient and did not lead to any reaction, although, as expected, increasing the temperature leads to more reactions. Over the total of 8000 simulations for each temperature, branching ratio were computed over efficient trajectories, considering 108 reactions at 80K, 201 at 250K, 251 at 300K, 314 at 350K and 517 at 800K. Figure 7 presents an example of one trajectory along the abstraction of one hydrogen atom in ortho position. The results are presented in the table VI.

With ReaxFF, due to the lack of π arrangement description, the addition of the OH is rare. So, we compare the rate constant of the H-abstraction reactions and the chloride substitution computed by Bryukov *et al.*[69] with those obtained in our ReaxFF simulations. Bryukov *et al.*[69] computed the rate constant with different methods, but the IRTS (Isodesmic reactions for transition states) shows the best capacity to reproduce the experimental results[71,72].

The lowest temperature investigated by Bryukov *et al.*[69] is 251.68K. At this temperature, the rate constants scale is as follows: the smallest is the chlorine substitution; the H-abstraction in para and ortho positions are one order of magnitude larger, the H-abstraction in ortho being favoured; finally, the H-abstraction in meta position is the kinetic product with a rate constant one order

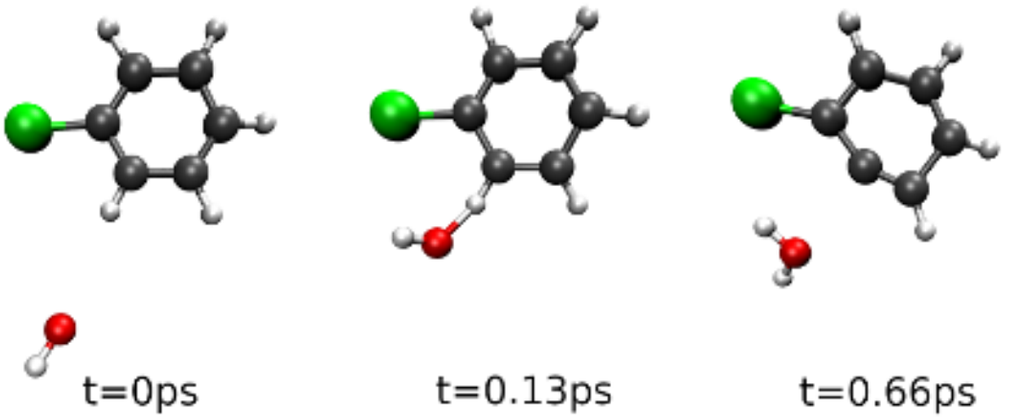

FIG. 7. Representation of key snapshots along one reaction pathway leading to the abstraction of an hydrogen atom in ortho position. The molecules are depicted on the different graphics with the chlorine atom in green, carbon in grey, hydrogen in white and oxygen in red.

Products	80K	250K	300K	350K	800K
Ortho abstraction	32.4	38.3	41.4	42.7	39.5
Meta abstraction	49.1	46.3	34.3	31.9	25.7
Para abstraction	9.3	8.5	13.6	12.4	6.4
Cl Substitution	9.3	6.5	8.8	12.4	24.2
HOCl Formation	-	0.5	2.0	0.6	4.1
Para OH addition	-	-	-	-	0.2

TABLE VI. Branching ratio (in %) over the efficient trajectory of a hydroxyl radical collision with chlorobenzene at 80K, 250K, 300K, 350K and 800K, obtained with ReaxFF and the CHONCl-2022_weak force field.

of magnitude larger than the ortho and para cases. These results agree with the branching ratio presented in table VI. The H-abstraction in the meta position is the more probable, while the chlorine substitution is unlikely to occur. However, the efficiency of the H-abstraction in ortho and para positions is not well reproduced, although they are effectively less probable than the meta H-abstraction. These results might come from the geometry of the complex between the OH

radical and the chlorobenzene molecule, far away from the transition state which are not included in the calculations done by Bryukov *et al.*[69]. From our QM calculations, the OH radical comes first between two carbon atoms before it reaches the transition state. Looking at the energy of the transition states on figure 6, the ortho position is favoured against the ipso position, the meta position is favoured against the para position, and the meta position is favoured against the ortho position. This is consistent with the branching ratio obtained in table VI. The calculations of the rate constants by including a two steps model with the approach of the hydroxyl radical may help to consider that point.

Increasing the temperature leads to a balance shift between the reaction pathway on positions ortho and meta, the para position remaining disfavored and the chloride atom substitution being more and more likely to occur. Bryukov *et al.*[69] showed that increasing the temperature reduces the difference between the rate constants of the chloride atom substitution and the three reaction pathways associated with the H-abstraction. The chloride atom substitution becomes prominent above 2343.75 K[69]. Although our ReaxFF simulations with CHONCl-2022_weak slightly overestimate this substitution pathways they agree with the trend of this reaction pathway to become favoured by increasing the temperature. Moreover, these results are consistent with reaction pathways calculations, on figure 6, where the chloride atom substitution corresponds effectively to the thermodynamic product, whatever the QM or ReaxFF calculation level.

The approach presented here, averaging molecular collisions using ReaxFF simulations, may help investigate atmospheric reactions using a few calculation times. ReaxFF results being reliable, such collision analyses may help probe the possible reactive pathways quickly and gather the possible reaction products.

C. Plasma-induced degradation of chlorobenzene in water

Finally, in order to demonstrate our new potential's capability, simulations corresponding to plasma-induced degradation of chlorobenzene in water were implemented with the CHONCl-2022_weak force field. To that ends, we considered a simulation box, of 15 length, containing one chlorobenzene molecule, 102 water molecules and 10 hydroxyl radicals to mimic the effect of the plasma. All compounds were randomly positioned in the box. The box was heated between 550 K and 750 K to fasten the reaction during 2 ns. A total of 35 simulations were made, and the results were compared to those obtained from the experimental investigation of Liu and Jiang[73].

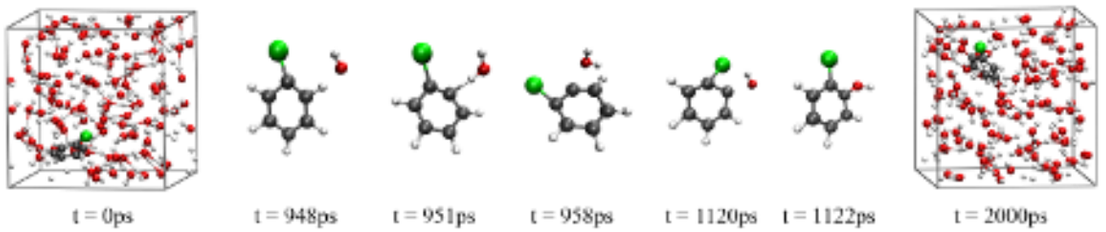

FIG. 8. Initial and last simulation boxes of the plasma-induced reactivity of chlorobenzene in water along with intermediate key snapshots of the reaction pathway and their corresponding timestep.

Figure 8, presents an example of a simulation box at the first time step and at the last one, along with key snapshots illustrating the reactivity along one simulation.

Among the 35 simulations, the degradation of chlorobenzene only occur in two cases. One leads to the formation of a phenol molecule and the other one leads to a chlorophenol molecule, the hydroxyl radical being crafted on the ortho position. Figure 8 presents the formation of the chlorophenol molecule. These results agree with the conclusions of Liu and Jiang [73] who showed from plasma-induced experiments that the main intermediates products of the chlorobenzene decomposition are the three chlorophenols and the phenol compounds. This opens the field of application of CHONCl-2022_weak force field to the investigation of organochloride decomposition from plasma-induced degradation in water.

IV. CONCLUSION

In this work, we developed a new reactive potential in the ReaxFF formalism called CHONCl-2022_weak force field. It provides the chlorine atom parameters for organochloride compounds to the CHON-2017_weak force field and focuses on conjugated and aromatic compounds. The force field parameters were fitted against high-level quantum mechanics calculations, including CASSCF/CASPT2 calculations for bond dissociation and DFT calculations for PESs along internal coordinates or reaction pathways. Its performance was evaluated against a validation set. We obtained an RMSD against QM energies of 0.38 eV (8.91 kcal mol^{-1}). Moreover, the RMSD over structural parameters of the new force field is 0.06Å for the bond lengths, 11.86° for the angles and 4.12° for the dihedral angles. The bond dissociation energies and PESs along bending and dihedral angles, computed at a QM level, are well reproduced. Moreover, the central torsion angle of molecules from the PCB family agree well with reference values from a structural and energetic

point of view which is of great interest as this torsion is a key factor in the toxicity of these compounds. Finally, the charge distribution over PCB molecules, computed with the new force field agrees with the one computed at the DFT level, allowing the identification of favourable zones for reactive nucleophilic addition on these compounds.

The atmospheric oxidation of the chlorobenzene molecule initiated by hydroxyl radical was investigated with the new force field and compared with DFT calculations. Two main reaction pathways were investigated: the addition of the OH radical on the chlorobenzene and the abstraction of one hydrogen atom or the substitution of the chlorine atom by the radical. Although ReaxFF tends to overestimate the energy barriers, the new force field reproduces the trends of QM results. The energy barriers of the two considered pathways are very closed. The reaction on the ipso position exhibits the largest energy barrier but leads to the lowest energy products. Considering the presence of a dixoygen molecule, the new force field reproduces the formation of chlorophenol and highly oxygenated molecules. To further increase the accuracy of the calculations, it could be needed to consider a better description of the π-stacking interaction in order to improve the interaction between the aromatic ring and the OH radical.

The regioselectivity associated with the reaction with an OH radical was also compared to rate constant calculations. Using an original approach, we simulated the atmospheric collisions between the chlorobenzene molecule and the OH radical and gathered statistical data to analyze the more probable reaction pathways. Again, the results obtained with the CHONCl-2022_weak force field agree with the literature, and we evidence the shift between the H-abstraction and the chloride atom substitution when increasing the temperature. This opens the possibility of probing reaction pathways and identifying reaction products quickly.

Finally, the degradation of chlorobenzene in water from the reaction with hydroxyl radicals was investigated using the CHONCl-2022_weak force field. The formation of phenol and chlorophenol molecules is obtained which agree with experimental investigation which identified these molecules as the major intermediates. This opens the filed of application of reactive molecular dynamic simulations using ReaxFF to the investigation of the degradation of organochloride compounds in water.

SUPPLEMENTARY MATERIAL

Supplementary material is available and provides (i) computational details about CASSCF/CASPT2 calculations (ii) density of several solvents computed with ReaxFF (iii) the structure and nomenclature of PCBs and (iv) reaction energies used to obtain the parameters. An archive is provided including data files, in the usual format for parameters optimization with AMS, containing the energies and the structures used to build the training set and the validation set and the force field parameters in a suitable format for LAMMPS or AMS.

ACKNOWLEDGMENTS

This work was achieved using HPC ressources from GENCI-CINES (grant `2021-A0100806920`), MCIA (Mésocentre de Calcul Intensif Aquitain) and the Université de Pau et des Pays de l'Adour.

REFERENCES

[1]A. C. T. van Duin, S. Dasgupta, F. Lorant, and W. A. Goddard, The Journal of Physical Chemistry A **105**, 9396 (2001).

[2]T. P. Senftle, S. Hong, M. M. Islam, S. B. Kylasa, Y. Zheng, Y. K. Shin, C. Junkermeier, R. Engel-Herbert, M. J. Janik, H. M. Aktulga, T. Verstraelen, A. Grama, and A. C. T. v. Duin, npj Computational Materials **2**, 1 (2016).

[3]K. Chenoweth, A. C. T. van Duin, P. Persson, M.-J. Cheng, J. Oxgaard, and W. A. Goddard, The Journal of Physical Chemistry C **112**, 14645 (2008).

[4]S. Monti, A. Corozzi, P. Fristrup, K. L. Joshi, Y. K. Shin, P. Oelschlaeger, A. C. T. v. Duin, and V. Barone, Physical Chemistry Chemical Physics **15**, 15062 (2013).

[5]W. Zhang and A. C. T. van Duin, The Journal of Physical Chemistry B **121**, 6021 (2017), publisher: American Chemical Society.

[6]W. Zhang and A. C. T. van Duin, The Journal of Physical Chemistry B **122**, 4083 (2018).

[7]O. R. Gittus and F. Bresme, The Journal of Chemical Physics **155**, 114501 (2021), publisher: American Institute of Physics.

[8]L. Shi, Z. Ying, A. Xu, and Y. Cheng, Physical Chemistry Chemical Physics **22**, 2978 (2020), publisher: The Royal Society of Chemistry.

[9]D. Dong, W. Zhang, A. Barnett, J. Lu, A. C. T. Van Duin, V. Molinero, and D. Bedrov, Polymers **10**, 1289 (2018), number: 11 Publisher: Multidisciplinary Digital Publishing Institute.

[10]U. Ali, J. H. Syed, R. N. Malik, A. Katsoyiannis, J. Li, G. Zhang, and K. C. Jones, Science of The Total Environment **476-477**, 705 (2014).

[11]G. M. E. Zokm, M. M. Ismail, and M. A. E. Okbah, Environmental Science and Pollution Research (2022), 10.1007/s11356-022-18634-z.

[12]O. M. Okeagu, B. Akinsanya, P. O. Isibor, J. Daniel-Rugu, A. B. Onadeko, B. Yalwaji, and K. O. Adekoya, Toxicology Reports **9**, 136 (2022).

[13]C. Keswani, H. Dilnashin, H. Birla, P. Roy, R. K. Tyagi, D. Singh, V. D. Rajput, T. Minkina, and S. P. Singh, Environmental Geochemistry and Health **44**, 149 (2022).

[14]Y. Ding, H. Huang, W. Chen, Y. Zhang, W. Chen, X. Xing, and S. Qi, Journal of Environmental Sciences **115**, 453 (2022).

[15]W. Chen, B. Peng, H. Huang, Y. Kuang, Z. Qian, W. Zhu, W. Liu, Y. Zhang, Y. Liao, X. Zhao, H. Zhou, and S. Qi, International Journal of Environmental Research and Public Health **19**, 263 (2022), number: 1 Publisher: Multidisciplinary Digital Publishing Institute.

[16]A. F. Veludo, D. Martins Figueiredo, C. Degrendele, L. Masinyana, L. Curchod, J. Kohoutek, P. Kukučka, J. Martiník, P. Přibylová, J. Klánová, M. A. Dalvie, M. Röösli, and S. Fuhrimann, Chemosphere **289**, 133162 (2022).

[17]G. A. Idowu, A. F. Aiyesanmi, and F. O. Oyegoke, Environmental Advances **7**, 100162 (2022).

[18]"AMAP Assessment 2002: The Influence of Global Change on Contaminant Pathways to, within, and from the Arctic,".

[19]UNEP, (2011).

[20]Z. Singh, American Journal of BioScience **4**, 11 (2016).

[21]R. Jayaraj, P. Megha, and P. Sreedev, Interdisciplinary Toxicology **9**, 90 (2016).

[22]S. Chen, Z. Han, D. Zhang, and J. Zhan, RSC Advances **4**, 52415 (2014), publisher: The Royal Society of Chemistry.

[23]K. Breivik, A. Sweetman, J. M. Pacyna, and K. C. Jones, Science of The Total Environment **377**, 296 (2007).

[24]D. Mackay, *Multimedia Environmental Models: The Fugacity Approach, Second Edition*, 2nd ed. (2001).

[25]M. M. Ododo and B. K. Wabalo, Journal of Environment Pollution and Human Health , 6 (2019).

[26]Van den Berg M, Birnbaum L, Bosveld A T, Brunström B, Cook P, Feeley M, Giesy J P, Hanberg A, Hasegawa R, Kennedy S W, Kubiak T, Larsen J C, van Leeuwen F X, Liem A K, Nolt C, Peterson R E, Poellinger L, Safe S, Schrenk D, Tillitt D, Tysklind M, Younes M, Waern F, and Zacharewski T, Environmental Health Perspectives **106**, 775 (1998), publisher: Environmental Health Perspectives.

[27]J. Padmanabhan, R. Parthasarathi, V. Subramanian, and P. K. Chattaraj, Journal of Molecular Structure: THEOCHEM **730**, 221 (2005).

[28]I. Ali, O. M. L. Alharbi, Z. A. Alothman, and A. Alwarthan, Environmental Research **160**, 353 (2018).

[29]J. Bai, W. Yang, C. Zhang, Y. Zhao, C. Gong, X. Sun, Q. Zhang, and W. Wang, Atmospheric Environment **67**, 177 (2013).

[30]C. M. Kao, S. C. Chen, J. K. Liu, and M. J. Wu, Chemosphere **44**, 1447 (2001).

[31]W. Wang, Y. Wang, W. Feng, W. Wang, and P. Li, Molecules **23**, 2826 (2018), number: 11 Publisher: Multidisciplinary Digital Publishing Institute.

[32]Z. Wen, Z. Wang, J. Xu, Y. Liu, and K. Cen, Chemosphere **92**, 293 (2013).

[33]N. Rashidian, E. Zahedi, and A. Shiroudi, Science of The Total Environment **679**, 106 (2019).

[34]Z. Liao, M. Zeng, and L. Wang, Chemosphere **240**, 124756 (2020).

[35]J. Hur, Y. N. Abousleiman, K. L. Hull, and M. J. A. Qomi, RSC Advances **11**, 29298 (2021), publisher: Royal Society of Chemistry.

[36]M. A. Wood, A. C. T. van Duin, and A. Strachan, The Journal of Physical Chemistry A **118**, 885 (2014), publisher: American Chemical Society.

[37]N. Hansen, S. D. Müller, and P. Koumoutsakos, Evolutionary Computation **11**, 1 (2003).

[38]G. te Velde, F. M. Bickelhaupt, E. J. Baerends, C. Fonseca Guerra, S. J. A. van Gisbergen, J. G. Snijders, and T. Ziegler, J. Comput. Chem. **22**, 931 (2001).

[39]Computer Physics Communications **271**, 108171 (2022).

[40]B. O. Roos, P. R. Taylor, and P. E. M. Sigbahn, Chemical Physics **48**, 157 (1980).

[41]B. Roos, R. Lindh, P. Malmqvist, V. Veryazov, and P.-O. Widmark, *Multiconfigurational Quantum Chemistry*, Multiconfigurational Quantum Chemistry (2016) pages: 224.

[42]C. Angeli, B. Bories, A. Cavallini, and R. Cimiraglia, The Journal of Chemical Physics **124**, 054108 (2006), publisher: American Institute of Physics.

[43]F. Neese, WIREs Computational Molecular Science **2**, 73 (2012).

[44]R. A. Kendall, T. H. Dunning, and R. J. Harrison, The Journal of Chemical Physics **96**, 6796 (1992), publisher: American Institute of Physics.

[45]M. J. Frisch, G. W. Trucks, H. B. Schlegel, G. E. Scuseria, M. A. Robb, J. R. Cheeseman, G. Scalmani, V. Barone, G. A. Petersson, H. Nakatsuji, X. Li, M. Caricato, A. V. Marenich, J. Bloino, B. G. Janesko, R. Gomperts, B. Mennucci, H. P. Hratchian, J. V. Ortiz, A. F. Izmaylov, J. L. Sonnenberg, D. Williams-Young, F. Ding, F. Lipparini, F. Egidi, J. Goings, B. Peng, A. Petrone, T. Henderson, D. Ranasinghe, V. G. Zakrzewski, J. Gao, N. Rega, G. Zheng, W. Liang, M. Hada, M. Ehara, K. Toyota, R. Fukuda, J. Hasegawa, M. Ishida, T. Nakajima, Y. Honda, O. Kitao, H. Nakai, T. Vreven, K. Throssell, J. A. Montgomery, Jr., J. E. Peralta, F. Ogliaro, M. J. Bearpark, J. J. Heyd, E. N. Brothers, K. N. Kudin, V. N. Staroverov, T. A. Keith, R. Kobayashi, J. Normand, K. Raghavachari, A. P. Rendell, J. C. Burant, S. S. Iyengar, J. Tomasi, M. Cossi, J. M. Millam, M. Klene, C. Adamo, R. Cammi, J. W. Ochterski, R. L. Martin, K. Morokuma, O. Farkas, J. B. Foresman, and D. J. Fox, "Gaussian~16 Revision C.01," (2016), gaussian Inc. Wallingford CT.

[46]A. D. Becke, The Journal of Chemical Physics **98**, 5648 (1993), publisher: American Institute of Physics.

[47]C. Lee, W. Yang, and R. G. Parr, Physical Review B **37**, 785 (1988), publisher: American Physical Society.

[48]S. H. Vosko, L. Wilk, and M. Nusair, Canadian Journal of Physics **58**, 1200 (1980), publisher: NRC Research Press.

[49]P. J. Stephens, F. J. Devlin, C. F. Chabalowski, and M. J. Frisch, The Journal of Physical Chemistry **98**, 11623 (1994), publisher: American Chemical Society.

[50]T. Clark, J. Chandrasekhar, G. W. Spitznagel, and P. V. R. Schleyer, Journal of Computational Chemistry **4**, 294 (1983).

[51]G. A. Petersson, A. Bennett, T. G. Tensfeldt, M. A. Al-Laham, W. A. Shirley, and J. Mantzaris, The Journal of Chemical Physics **89**, 2193 (1988), publisher: American Institute of Physics.

[52]G. A. Petersson and M. A. Al-Laham, The Journal of Chemical Physics **94**, 6081 (1991), publisher: American Institute of Physics.

[53]S. Grimme, S. Ehrlich, and L. Goerigk, Journal of Computational Chemistry **32**, 1456 (2011), _eprint: https://onlinelibrary.wiley.com/doi/pdf/10.1002/jcc.21759.

[54]M. Rajzmann, J. Wang, and S. Humbel, Molecular Catalysis **443**, 148 (2017).

[55]M. Head-Gordon, J. A. Pople, and M. J. Frisch, Chemical Physics Letters **153**, 503 (1988).

[56]S. Sæbø and J. Almlöf, Chemical Physics Letters **154**, 83 (1989).

[57]M. J. Frisch, M. Head-Gordon, and J. A. Pople, Chemical Physics Letters **166**, 281 (1990).

[58]M. J. Frisch, M. Head-Gordon, and J. A. Pople, Chemical Physics Letters **166**, 275 (1990).

[59]M. Head-Gordon and T. Head-Gordon, Chemical Physics Letters **220**, 122 (1994).

[60]S. Nosé, The Journal of Chemical Physics **81**, 511 (1984), publisher: American Institute of Physics.

[61]W. G. Hoover, Physical Review A **31**, 1695 (1985), publisher: American Physical Society.

[62]D. Furman and D. J. Wales, The Journal of Physical Chemistry Letters **10**, 7215 (2019), publisher: American Chemical Society.

[63]J. McKinney and P. Singh, Chemico-Biological Interactions **33**, 271 (1981).

[64]O. Bastiansen and S. Samdal, Journal of Molecular Structure **128**, 115 (1985).

[65]S. Arulmozhiraja and T. Fujii, The Journal of Chemical Physics **115**, 10589 (2001), publisher: American Institute of Physics.

[66]T. I. Gorbunova, J. O. Subbotina, V. I. Saloutin, and O. N. Chupakhin, Journal of Hazardous Materials **278**, 491 (2014).

[67]O. V. Dorofeeva, V. P. Novikov, N. F. Moiseeva, and V. S. Yungman, Journal of Molecular Structure: THEOCHEM **637**, 137 (2003).

[68]R. Wu, S. Wang, and L. Wang, Chemosphere **111**, 537 (2014).

[69]M. G. Bryukov, V. D. Knyazev, W. M. Gehling, and B. Dellinger, The Journal of Physical Chemistry A **113**, 10452 (2009), publisher: American Chemical Society.

[70]M. Priestley, T. J. Bannan, M. Le Breton, S. D. Worrall, S. Kang, I. Pullinen, S. Schmitt, R. Tillmann, E. Kleist, D. Zhao, J. Wildt, O. Garmash, A. Mehra, A. Bacak, D. E. Shallcross, A. Kiendler-Scharr, A. M. Hallquist, M. Ehn, H. Coe, C. J. Percival, M. Hallquist, T. F. Mentel, and G. McFiggans, Atmospheric Chemistry and Physics **21**, 3473 (2021).

[71]V. D. Knyazev, The Journal of Physical Chemistry A **106**, 11603 (2002), publisher: American Chemical Society.

[72]V. D. Knyazev, The Journal of Physical Chemistry A **107**, 11082 (2003), publisher: American Chemical Society.

[73]Y. Liu and X. Jiang, Plasma Chem. Plasma Process. **28**, 15 (2008).